JGP Journal of General Physiology

RESEARCH ARTICLE

The central role of the tail in switching off 10S myosin II activity

Shixin Yang[1*], Kyoung Hwan Lee[1*], John L. Woodhead[1], Osamu Sato[2], Mitsuo Ikebe[2], and Roger Craig[1]

Myosin II is a motor protein with two heads and an extended tail that plays an essential role in cell motility. Its active form is a polymer (myosin filament) that pulls on actin to generate motion. Its inactive form is a monomer with a compact structure (10S sedimentation coefficient), in which the tail is folded and the two heads interact with each other, inhibiting activity. This conformation is thought to function in cells as an energy-conserving form of the molecule suitable for storage as well as transport to sites of filament assembly. The mechanism of inhibition of the compact molecule is not fully understood. We have performed a 3-D reconstruction of negatively stained 10S myosin from smooth muscle in the inhibited state using single-particle analysis. The reconstruction reveals multiple interactions between the tail and the two heads that appear to trap ATP hydrolysis products, block actin binding, hinder head phosphorylation, and prevent filament formation. Blocking these essential features of myosin function could explain the high degree of inhibition of the folded form of myosin thought to underlie its energy-conserving function in cells. The reconstruction also suggests a mechanism for unfolding when myosin is activated by phosphorylation.

Introduction

Myosin II is a motor protein that, together with actin filaments, generates mechanical force and motion using the chemical energy of ATP hydrolysis (Geeves and Holmes, 1999). In muscle, myosin II is responsible for shortening and force production, while in nonmuscle cells, it is essential in cell adhesion and division, intracellular transport, and cell migration (Vicente-Manzanares et al., 2009; Shutova and Svitkina, 2018). The myosin II molecule is a hexamer composed of two heavy chains, two essential light chains (ELCs), and two regulatory light chains (RLCs). The light chains and the N-terminal halves of the heavy chains form two globular heads, containing ATP- and actin-binding sites, while the heavy chain C-terminal halves form an α-helical coiled-coil tail extending from the heads. The tails self-associate to form the backbone of thick filaments, which are the functional form of myosin II in muscle and cell motility. Mutations in the heads and tail impair myosin function and cause diseases in muscle and other cells (Vicente-Manzanares et al., 2009; Moore et al., 2012; Tajsharghi and Oldfors, 2013; Newell-Litwa et al., 2015). Myosin II molecules can exist in two conformations, 6S and 10S, named for their sedimentation coefficients (Suzuki et al., 1978). 10S molecules have a compact structure in which the tail is folded into three segments of similar length, and the heads are bent back on the tail and interact with each other (Fig. 1; Suzuki et al., 1982; Trybus et al., 1982; Craig et al., 1983; Burgess et al., 2007; Jung et al., 2008b). This folded conformation traps the products of ATP hydrolysis, causing strong inhibition of ATPase activity (Cross et al., 1986) and inhibiting assembly into thick filaments. Phosphorylation of the RLC in 10S molecules favors unfolding to the 6S form (Craig et al., 1983; Trybus and Lowey, 1984; Cross, 1988), in which ATPase activity is switched on (Sellers, 1991), and the tail has an extended conformation, favoring filament assembly.

The inhibited, 10S molecule is thought to play a fundamental role in nonmuscle cells, where it appears to serve as an energy-conserving, storage form of myosin and to provide assembly units for thick filament formation when and where contractile activity is required (Cross, 1988; Breckenridge et al., 2009; Milton et al., 2011; Kiboku et al., 2013; Heissler and Sellers, 2016; Liu et al., 2017; Shutova and Svitkina, 2018). Its compact conformation is thought to facilitate transport to the sites of filament assembly and thus motility (Breckenridge et al., 2009; Kiboku et al., 2013). The 10S molecule may also play a role in the

[1]Division of Cell Biology and Imaging, Department of Radiology, University of Massachusetts Medical School, Worcester, MA; [2]Department of Cellular and Molecular Biology, University of Texas Health Science Center at Tyler, Tyler, TX.

*S. Yang and K.H. Lee contributed equally to this paper; Correspondence to Roger Craig: roger.craig@umassmed.edu; K.H. Lee's present address is Massachusetts Facility for High-Resolution Cryo-Electron Microscopy, University of Massachusetts Medical School, Worcester, MA. A non-peer-reviewed preprint of this paper was posted in *bioRxiv* on April 11, 2019.

© 2019 Yang et al. This article is distributed under the terms of an Attribution–Noncommercial–Share Alike–No Mirror Sites license for the first six months after the publication date (see http://www.rupress.org/terms/). After six months it is available under a Creative Commons License (Attribution–Noncommercial–Share Alike 4.0 International license, as described at https://creativecommons.org/licenses/by-nc-sa/4.0/).

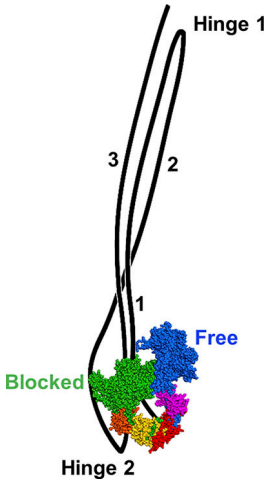

Figure 1. **Model of 10S myosin.** Blocked head consists of heavy chain (green), ELC (orange), and RLC (yellow). Free head shows heavy chain (blue), ELC (magenta), and RLC (red). The tail is folded into three segments: segment 1 (subfragment 2), originating from the heads and ending at hinge 1; segment 2, starting at hinge 1 and ending at hinge 2; and segment 3, starting at hinge 2 and ending at the tip of the tail. Based on Burgess et al. (2007) and Lee et al. (2018).

function of some smooth muscles, by providing a pool of inactive monomers that can unfold and augment myosin filament length or number when smooth muscle is activated (Xu et al., 1997; Seow, 2005; Milton et al., 2011). In striated muscles, myosin is almost exclusively filamentous, but there is nevertheless a small concentration of soluble myosin whose compact form has been proposed to facilitate transport to sites of filament assembly during muscle development and myosin filament turnover (Ankrett et al., 1991; Katoh et al., 1998; Takahashi et al., 1999).

A unique structural feature of 10S myosin is an asymmetric interaction between its two heads (the interacting-heads motif, or IHM), which inhibits their activity (Wendt et al., 2001). Head–head interaction was first observed in 2-D crystals of smooth muscle heavy meromyosin (HMM) in the switched-off state (RLCs dephosphorylated; Wendt et al., 2001) and later confirmed by EM and 2-D classification of single myosin II molecules (Burgess et al., 2007). Inhibition was suggested to occur by different mechanisms in the two heads. In one head (blocked), actin binding is hindered by proximity of the other head (free) to its actin-binding site. In contrast, ATPase activity of the free head is inhibited through stabilization of its converter domain interacting with the blocked head (Wendt et al., 2001). 3-D reconstruction of thick filaments subsequently showed that 6S myosin, when polymerized into thick filaments, has a similar head–head interaction to that in folded, 10S molecules (Woodhead et al., 2005). The IHM in thick filaments may underlie the super-relaxed state of muscle (Stewart et al., 2010), in which myosin activity is highly inhibited, thus serving as an important energy-conserving mechanism for striated muscle.

The IHM structure has been compared in a variety of evolutionarily diverse species. EM and 2-D image classification of negatively stained molecules shows that the compact, folded form of 10S myosin has been conserved since the origin of animals, with head–head interactions in the IHM appearing similar in all species studied (Jung et al., 2008a,b; Lee et al., 2018). Similarly, the IHM first observed in thick filaments in cryo-EM studies of tarantula muscle (Woodhead et al., 2005) has been confirmed in thick filaments from a variety of vertebrate and invertebrate species (Zoghbi et al., 2008; Zhao et al., 2009; Pinto et al., 2012; Woodhead et al., 2013). The high level of conservation of the IHM in isolated molecules and thick filaments over hundreds of millions of years suggests that it is a fundamental structure, critical to the function of muscle and nonmuscle cells (Jung et al., 2008a,b; Lee et al., 2018).

While the inhibitory interactions between the heads in the IHM are similar in thick filaments and 10S molecules, the activity of the 10S molecule is inhibited an order of magnitude more than myosin in thick filaments (Cross et al., 1988; Ankrett et al., 1991). Additional interactions with the folded tail occurring in 10S myosin but not in filaments may account for this difference. However, it is not known what these interactions might be, as no 3-D reconstruction of the entire 10S molecule has been reported. The interactions between the heads in 10S myosin were well defined in cryo-EM studies of 2-D crystals (Liu et al., 2003), but the tail was poorly visualized, and the 3-D reconstruction provided no insights into its potential role in regulation. The tail (as well as the heads) was clearly delineated in 2-D class averages of negatively stained, isolated 10S molecules, but its course in three dimensions was not studied (Burgess et al., 2007). Here we present a 3-D reconstruction of 10S myosin molecules using negative staining and single-particle analysis. The reconstruction clearly reveals the 3-D course of the tail as it wraps around the heads, showing evidence for interaction with the heads at eight sites and suggesting mechanistic bases for the inhibition of the four key elements of myosin II function: actin binding, ATPase activity, RLC phosphorylation, and filament assembly. The results provide a structural model for the total shutdown of myosin II activity when in its compact, energy-conserving 10S form.

Materials and methods

Electron microscopy

Smooth muscle myosin II from turkey gizzard was purified according to Ikebe and Hartshorne (1985). Smooth muscle myosin has similar structural and functional properties to nonmuscle myosin II (including formation of the folded structure; Craig et al., 1983) and is a convenient source for our experiments on the 10S conformation. Myosin molecules in 0.15 M NaAc, 1 mM EGTA, 2.5 mM $MgCl_2$, 0.5 mM ATP, and 10 mM MOPS, pH 7.5, were negatively stained at 10 nM concentration using 1% (wt/vol) uranyl acetate (Takizawa et al., 2017). Carbon films were pretreated with UV light to optimize stain spreading (Burgess et al., 2004; Jung et al., 2008b). The 10S structure is formed by relatively weak interactions that can be disrupted by EM preparative conditions (Jung et al., 2011; Lee et al., 2018). To avoid this possibility, molecules were lightly cross-linked in solution at room temperature for 1 min with 0.1% glutaraldehyde before staining (Jung et al., 2008b, 2011). This treatment does not significantly alter the structure of the molecules at the resolution of

our studies, but serves to stabilize that structure (Jung et al., 2008b, 2011), producing a more homogeneous population, which facilitates 3-D reconstruction. Glutaraldehyde has in fact been used to stabilize flexible proteins to 4.0-Å resolution in cryo-EM studies (Urnavicius et al., 2015). 200 micrographs were recorded under low-dose conditions on a Thermo Fisher Scientific (Philips) CM120 transmission electron microscope at 120 kV with a 2K × 2K charge-coupled device camera (F224HD; TVIPS) at a pixel size of 3.7 Å (nominal 45,000× magnification). These micrographs were used for 3-D reconstruction and refinement. 100 pairs of micrographs of tilted (50°) and untilted (0°) grids were collected at 5.4 Å/pixel (nominal magnification 37,000×) for random conical tilt reconstruction.

Image processing

Initial model from random conical tilt

No complete 3-D model is available for 10S myosin II to use as a reference for 3-D reconstruction. To exclude model bias, we implemented the random conical tilt method (Radermacher et al., 1987) to create a starting model, using SPIDER (Frank, 2006). 13,675 pairs of particles were interactively selected from the 100 tilted and untilted micrographs using the program JWEB in SPIDER. 2-D classification was performed for the untilted particles. Four classes of particle with similar views in the class averages were chosen for further analysis. For each class, the Euler angle of each particle from the tilt images was calculated based on the tilt angle and the azimuthal angle from 2-D classification. Back projection was performed to compute the 3-D reconstruction. Finally, the four class averages were rotated to make the tail parallel to the y axis. The azimuthal angles obtained were used to modify the Euler angles and to merge particles from the chosen four classes, and the model was built using the merged dataset.

2-D classification and 3-D reconstruction

The folded tail of 10S myosin protruding beyond the heads is flexible, and also rotates (within a 60° range) about its junction with the heads (Burgess et al., 2007). To simplify analysis, only particles with an unbent tail pointing straight up from the head–head junction were chosen for image processing. Particles with dimensions of 150 × 150 pixels, including both heads and a small portion of the protruding tail, were manually selected using EMAN (Tang et al., 2007) and then low-pass filtered to 20 Å. All subsequent image processing was performed with RELION (Scheres, 2012). Four rounds of 2-D classification were performed. Bad or low-resolution particles with smeared densities were removed after each round. The remaining 15,833 particles were subjected to 3-D classification into six classes using the 3-D reconstruction from random conical tilt, low-pass filtered to 50 Å, as the starting model. Classes 1, 2, and 5 showed variable appearances of the tail and heads. Classes 3 and 4 had similar 3-D reconstructions and were combined for refinement. Class 6 molecules showed less detail than classes 3 and 4 and were excluded from the final reconstruction.

Atomic fitting

The atomic model of the interacting heads of chicken smooth muscle myosin (PDB ID 1I84; Wendt et al., 2001) was docked into the 3-D reconstruction using rigid-body fitting in UCSF Chimera (Pettersen et al., 2004; Fig. 4). Molecular dynamics flexible fitting was not attempted owing to the low resolution. Densities outside of the heads were attributed to the three segments of the tail. According to 3-D classification (Fig. 6), subfragment 2 (S2) in the 3-D reconstruction was quite flexible. We therefore chose not to fit an atomic model of S2 to the reconstruction. Videos of the reconstruction and fitting were made using UCSF Chimera (Pettersen et al., 2004).

Online supplemental material

Fig. S1: 2-D class averages of negatively stained 10S myosin molecules. Fig. S2: Gold-standard Fourier shell correlation curve to determine resolution. Fig. S3: Location of initial portion of subfragment 2. Fig. S4: Comparison of low and high contour cutoff reconstructions to reveal stronger and weaker parts of the density. Fig. S5: Particle distribution of the six classes after 3-D classification. Fig. S6: Negatively stained insect indirect flight muscle and *Dictyostelium discoideum* myosin II. Fig. S7: Interaction of the RLC N-terminal with tail segment 3. Video 1: 3-D reconstruction of 10S smooth muscle myosin rotated about its long axis. Video 2: Atomic fitting of PDB ID 1I84 into the 3-D reconstruction of the 10S molecule. Video 3: Tail segment 3 contact with the RLC of the blocked head. Video 4: Steric blocking of Ser19 on the blocked head by tail segment 3.

Results

2-D class averages of 10S myosin

Turkey gizzard smooth muscle myosin at physiological ionic strength (0.15 M NaAc) in the presence of ATP was observed by negative staining with 1% uranyl acetate (Burgess et al., 2004; Takizawa et al., 2017). The compact, folded (10S) conformation dominated the EM images, with a small number of antiparallel 10S dimers, displaying a dumbbell-shaped structure (Fig. 2 A) and very few extended (6S) molecules. Only 10S monomers were chosen for image processing. The tail in these molecules was folded into three segments and wrapped around the heads, as previously described (Burgess et al., 2007). The heads showed different apparent shapes and sizes, corresponding to different orientations of the molecules on the EM grid (Fig. 2, B–E; and Fig. S1). Compared with the relatively rigid arrangement of the interacting heads, the tail was quite flexible where it extended away from the heads. In this region, segments 1, 2, and 3 (Fig. 1) run closely together, and this combined three-segment rod bends within a range of ∼60° from its point of emergence from the heads, as previously described (Burgess et al., 2007). Typical 2-D class averages of the interacting heads and the proximal portion of the three-segment tail are shown in Fig. 2 (B–E) and Fig. S1. The asymmetric architecture of the blocked and free heads was consistent with the results of previous 2-D classification analysis (Burgess et al., 2007; Jung et al., 2008a,b, 2011). Mirrored class averages, where molecules lie on the grid facing down or up, were observed as previously reported (Jung et al.,

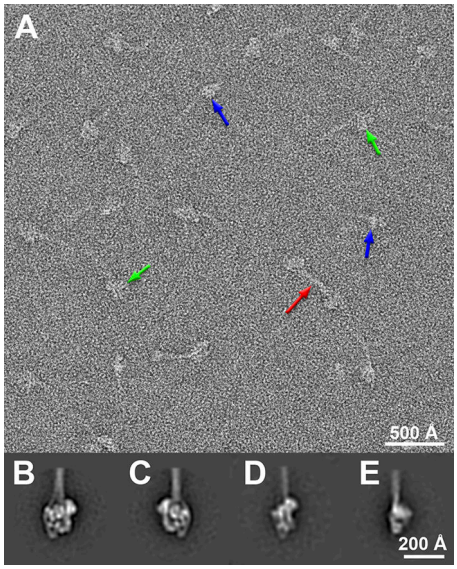

Figure 2. **Negatively stained 10S smooth muscle myosin molecules. (A)** Two types of structure are visible: monomers, in front and side views (green and blue arrows, respectively), and occasional dimers (red arrow). **(B–D)** 2-D class averages of right and left views (B and C, respectively; Jung et al. [2008b]); partially rotated view (D); and side view (E; see also Fig. S1).

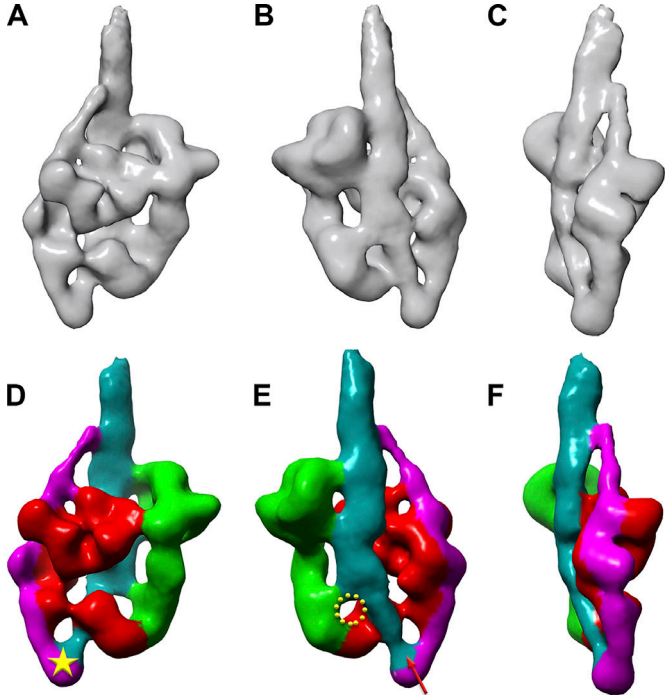

Figure 3. **3-D reconstruction of 10S smooth muscle myosin.** Electron Microscopy Databank accession code EMD-20084. **(A–C)** Front, back, and side views, respectively. **(D–F)** D–F correspond to A–C, with colors indicating different components of the structure. Blocked head is red; free head, green; tail segments 1 and 3, cyan; segment 2, magenta. In E, yellow circle indicates putative location of missing segment 1 density (see Fig. S3); red arrow, start of segment 3. Yellow star in D indicates the second hinge point.

2011; Fig. S1). The class averages showed that the myosin molecules typically lie parallel to the grid surface; the different orientations about their long axis enabled us to analyze the 3-D structure of the molecules using single-particle analysis.

3-D reconstruction

An initial 3-D structure of the folded molecule was computed using the random conical tilt method (Radermacher et al., 1987), in which images are recorded at 0° and 50° tilts. This model was then used for projection matching to determine the final single-particle reconstruction (Electron Microscopy Databank accession no. EMD-20084). Computing the initial structure ab initio excludes potential model bias in the results. The final reconstruction had a moderate resolution (25 Å; Fig. S2), limited by the flexibility of the molecule and the resolution limits of negative staining. This was sufficient to resolve domains as small as 10 kD, such as the N- and C-terminal lobes of the RLC (Burgess et al., 2004, 2007; Figs. 3 and 4).

The head region of the reconstruction had the appearance of a flat disk, with an irregular polygonal "front" view (as viewed in Fig. 3, A and D; and Video 1), enclosing a central hole, and a narrow side view (Fig. 3, C and F; and Video 1), similar to the interacting-head motifs seen in 2-D crystals of HMM and myosin (Wendt et al., 2001; Liu et al., 2003) and in thick filaments (Woodhead et al., 2005). The atomic model of the interacting-heads structure computed from cryo-imaged smooth muscle HMM 2-D crystals (PDB ID 1I84; Wendt et al., 2001) docked well into the reconstruction using rigid-body fitting (Fig. 4 and Video 2), confirming this similarity. This was clear in both front and side views (Fig. 4, D and F). The fit implies good preservation of the IHM in negatively stained single molecules (Takizawa et al., 2017), without significant flattening, and makes possible the identification of key features of the blocked and free heads in the reconstruction (Figs. 4 and 5).

The reconstruction also revealed the 3-D course of the folded tail as it wraps around the heads, a feature that was mostly missing from the only previous reconstruction of 10S myosin (Liu et al., 2003). Only a small portion of the region of the folded tail (~150 Å) that extends as three merged segments above the heads was included in the reconstruction, due to flexibility of the distal region. However, the essential part of the tail that interacts with the heads was included. Three segments of the tail could be identified in this region (Fig. 3). Strikingly, all three appear to bind to the heads: segment 2 along the left side of the blocked head (Figs. 1 and 3, A and D) and segments 1 and 3 on the back side of both heads (Fig. 3, B and E; and Video 1). Segment 1 (S2 of the tail) would be expected to start at the merge point of the lever arms of the blocked and free heads (blue ribbon, Fig. S3). However, there was missing density for this initial portion of subfragment 2 in the reconstruction (circle, Figs. 3 E and S3), a known issue for this very flexible region of the tail (Brown et al., 2008; Woodhead et al., 2013); more density becomes visible at low contour cutoff (Fig. S4). The first visible part of segment 1 density was assumed to occur where the tail density (cyan) widens, as segment 1 joins segment 3 (above the circle, Fig. 3 E). Segment 1 then runs next to segment 3 across the blocked head (in a region now known as the mesa; Spudich, 2015) toward the top, where segments 1 and 3 merge with

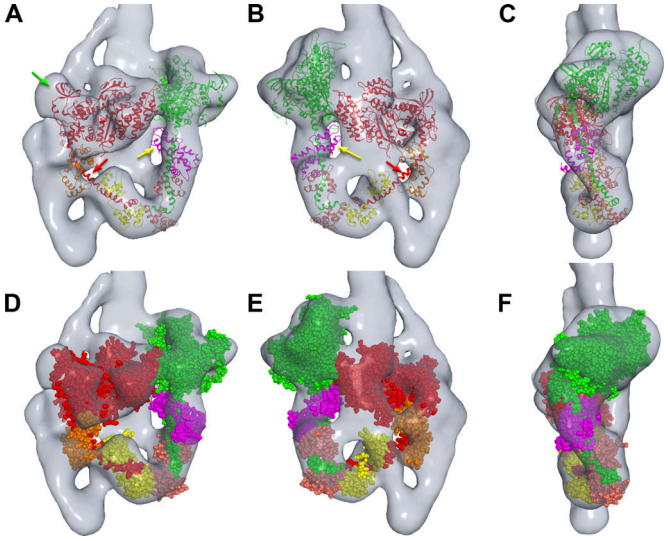

Figure 4. **Docking of atomic model of the IHM into the reconstruction.** The 2-D crystal model of smooth muscle myosin (PDB ID 1I84; Wendt et al., 2001) was used in the fitting. Molecular dynamics flexible fitting was not used, due to the low resolution. **(A–C)** Front, back, and side views, respectively, docked with ribbon representation of the atomic model. **(D–F)** D–F correspond to A–C, but with space-filling model. The atomic model fits well into the reconstruction in all views, except for the narrow part of the lever arm in the blocked head (single α-helix, between the two light chains; red arrow) and part of the ELC in the free head (yellow arrow). The low density in the reconstruction at these points may be due to extension of the stain pool that accumulates in the hole at the center of the IHM (cf. Figs. 2 B and S1) into these low-density regions of protein, obscuring them. Unfilled densities mostly represent portions of the three segments of the tail, for which there is no atomic model. There is also some unfilled density in the blocked head (green arrow) that would be filled by repositioning the flexibly connected SH3 domain (not done with the rigid-body docking procedure; see Materials and methods). In a previous study, molecular dynamics flexible fitting of cryo-imaged tarantula thick filaments demonstrated this point (Yang et al., 2016). Note: C and F rotated in opposite direction from C and F in Fig. 3.

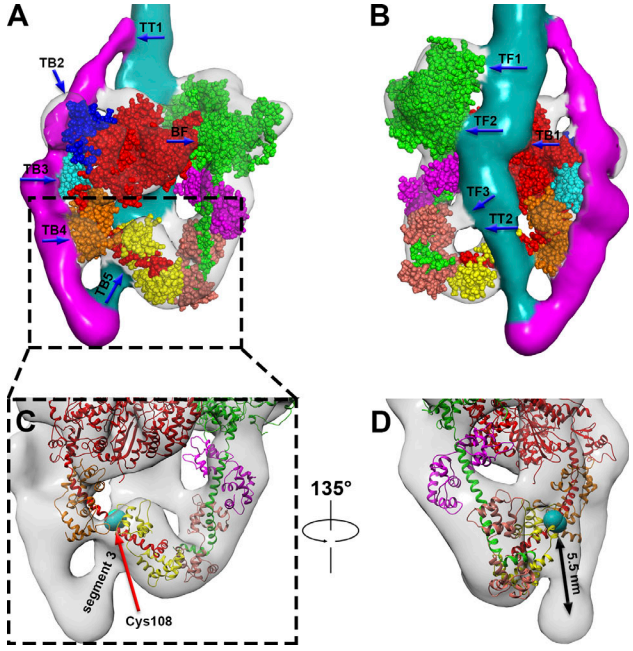

Figure 5. **Interactions between the tail and heads in 10S myosin. (A)** Front view of reconstruction fitted with PDB ID 1I84 shows the interactions between tail segments 2 (magenta) and 3 (cyan) and the blocked head (TB2, TB3, TB4, TB5), between the two heads (BF), and between segment 2 and the other tail segments (the interaction extends upwards from TT1). TB2 is between the SH3 domain (blue) in the blocked head and segment 2, lying underneath. TB3 is between segment 2 and the converter domain (cyan) of the blocked head. TB4 is between segment 2 and the ELC (orange) of the blocked head. TB5 is between segment 3 and the blocked-head RLC. **(B)** Back view shows the interaction between the free head and the tail (TF1, TF2, TF3), between segments 1 and 3 (unresolved from each other) and the blocked head (TB1), and between tail segments 1 and 3 (starting at TT2). Interaction TF1 is between the actin-binding loop in the free head and the tail, while TF2 is between the free head upper 50K domain and the tail. TF3 may represent merging of tail and blocked head densities and not be a real interaction (see Results). TB1 is an extended interaction between the blocked head and segment 1 and/or segment 3. **(C)** Magnified view of TB5. Cys108 is represented by a cyan sphere. **(D)** The view in C is rotated 135° to visualize the geometric relationship between Cys108 and segment 3.

segment 2 (Fig. 3, D and E). Segment 2 (magenta in Fig. 3) branches from the merged segments near the top and wraps around the blocked head. The end of this segment and the starting point of segment 3 form the second hinge point of the tail (Figs. 1 and 3 D), thought to occur at Glu1535 (Burgess et al., 2007). This region of density (marked with a star in Fig. 3 D) is unique to 10S myosin and is not found in HMM (lacking segments 2 and 3) or thick filaments (where the tail is unfolded). Segment 3 (red arrow in Fig. 3 E) starts from the hinge point, then runs, merged with segment 1, over the back of the blocked head (Fig. 3, D and E) to the top of the IHM, where they join segment 2. This arrangement of segments 1 and 3 on the same side (rather than opposite sides) of the IHM (Figs. 3 and 5), as also suggested from 2-D analysis (Burgess et al., 2007), would allow for rapid opening of the molecule upon activation.

Intramolecular interactions within 10S smooth muscle myosin molecules

The 3-D reconstruction and atomic fitting reveal key interactions occurring within the 10S myosin molecule (summarized in Table 1). Three types of interaction were found: head–head, head–tail, and tail–tail. The interaction between the blocked and free heads (BF) has been described before (Wendt et al., 2001; Liu et al., 2003) and is confirmed here. Eight putative interactions between the heads and the tail have not previously been observed in 3-D: these include the free head with tail segments 1 and 3 (TF), and the blocked head with tail segments 1, 2, and 3 (TB). Interactions between different segments of the tail were also observed (TT).

Head–head interactions

As described previously, the overall conformation of the IHM is produced by the blocked and free heads (red and green, respectively, in Fig. 3) interacting with each other (BF, blue arrow in Fig. 5 A; Wendt et al., 2001). The atomic model from this earlier work (PDB ID 1I84) can be fitted well into the volume (Fig. 4 and Video 2).

Table 1. **Summary of IHM interactions**

Interaction	Interacting components	Molecule/filament	Cartoon
BF	Blocked head, free head	10S, filament	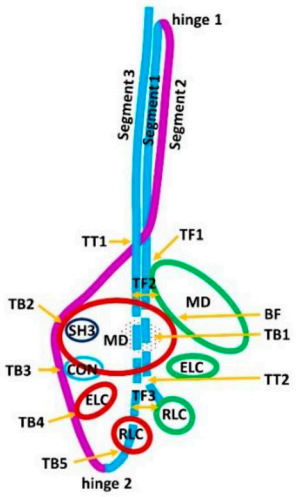
TB1	Segments 1 and 3, blocked head mesa	10S, filament	
TB2	Segment 2, blocked head SH3	10S, filament	
TB3	Segment 2, blocked head converter	10S, filament	
TB4	Segment 2, blocked head ELC	10S	
TB5	Segment 3, blocked head RLC	10S	
TF1	Segment 1 or 3, free head actin-binding loop	10S, filament	
TF2	Segment 1 or 3, free head ATPase loop 5	10S	
TF3	Segment 1 or 3, free head RLC	10S	
TT1	Segments 1, 2, 3	10S	
TT2	Segments 1, 3	10S	

The table and cartoon summarize the head–head, head–tail, and tail–tail interactions in 10S myosin, based on the 3-D reconstruction and fitting. The cartoon corresponds to the reconstruction in Fig. 5 (A and B). Blocked and free heads are represented by red and green, respectively. Yellow dots represent mesa of blocked head. CON, converter; MD, motor domain; SH3, SRC homology 3 domain. TT1 and TT2 mark initial points of contact between segments 1, 2, and 3 and segments 1 and 3, respectively. From these initial points, these segments run closely together and may interact along much of their lengths. Note: Corresponding domains in the two heads have different apparent shapes and sizes in this 2-D representation of the 3-D reconstruction, in which the domains are viewed at different angles (cf. Fig. 5 A).

Tail–head interactions

Three interactions are found between segment 2 of the tail and the blocked head as the tail wraps around its perimeter (Fig. 5 A). TB2 is the interaction between segment 2 and the blocked head SH3 domain (blue in Fig. 5 A). Interaction TB3 was found between segment 2 and the converter domain of the blocked head (cyan in Fig. 5 A). The third interaction, TB4, was found between segment 2 and the ELC of the blocked head (orange in Fig. 5 A).

Four interactions were observed between the tail and the underside of the heads (Fig. 5, A and B; and Table 1). TB1 is an extensive interaction, where the tail (including segments 1 and 3, which are not resolved from each other) runs over the back surface of the blocked head motor domain (Fig. 5 B). TB5 involves interaction between the RLC of the blocked head and segment 3, close to the second tail hinge point (Fig. 5 A). TF1 occurs between the tail and the actin-binding loop of the free head, while TF2 is the interaction between tail segment 1 or 3 and the upper 50K domain of the free head. TF3 is a possible interaction between the tail and the free-head RLC, but could alternatively represent low-resolution merging of densities without actual contact (Fig. S4; see Discussion). These interactions between the tail and the free head were not reported in 2-D analysis of smooth muscle myosin (Burgess et al., 2007; Jung et al., 2011), probably because the tail in these interactions is superimposed on the heads and cannot be identified in the 2-D projections.

Tail–tail interactions

In addition to the head–tail interactions, two regions of contact were found between the different segments of the tail. TT1 is an extensive interaction starting at the top of the IHM (Fig. 5 A), where segment 2 merges with segments 1 and 3, and continuing up as a triple coiled-coil complex (Burgess et al., 2007). A second extensive interaction appears likely between segments 1 and 3 (unresolved from each other), as they pass together over the blocked head (Fig. 5 B). This interaction starts at TT2, where the first part of segment 3 (cyan in Fig. 5 B) would merge with the initial portion of S2 (not visible in the reconstruction, as discussed earlier). Other parts of the tail (the region of segment 2 peeling away from the triple segment and wrapping around the blocked head, and the start of segment 3 after the second tail hinge) exist as single coiled coils, consistent with their narrower diameter in the reconstruction.

Heterogeneity in the reconstruction

The flexibility of the merged tail segments extending beyond the head region is visualized in raw images and was investigated using 2-D classification by Burgess et al. (2007), who showed that the tail flexed within a range of ∼60° where it left the heads. The heads are also flexible, although more rigid than the tail. 3-D classification was performed to explore flexibility and heterogeneity in the 10S molecules. 15,833 particles were classified into six classes using RELION (Scheres, 2012; Figs. 6 and S5). Classes 3 and 4, comprising 51% of the particles, exhibited very similar structures (Fig. 6, C and D). Both tail and IHM were visualized clearly in 3-D reconstructions and could be fitted well with the 3-D atomic model of chicken smooth muscle myosin. The particles in these classes were combined and used for 3-D refinement to produce the reconstruction described above. The other

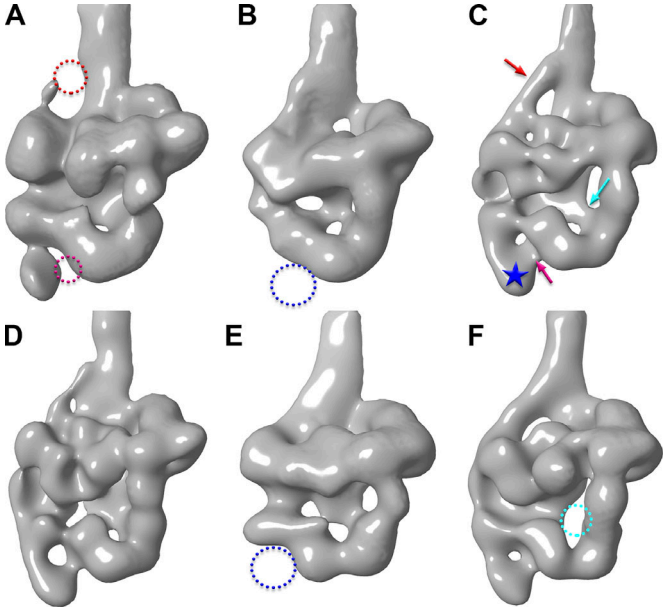

Figure 6. **Heterogeneity in the reconstruction.** 3-D classification using RELION produced six classes of conformation (A–F, classes 1–6, respectively), showing that the 10S myosin molecules are quite heterogeneous, due either to variable staining and/or other factors during specimen preparation or to natural variation in the molecules themselves. **(A)** The tail density partially disappeared in some regions (red dotted circles; cf. red arrow in C, where it is visible). **(B)** The tail cannot be explicitly identified in this reconstruction, and the second hinge point (star in C) is missing (blue circle). The reconstructions in C and D showed similar structural features, with both the interacting heads and the tail clearly visible. **(E)** Segment 2 around the blocked head is not visible, and the second hinge point is absent (blue circle), as in B. **(F)** The tail wraps around the blocked head, but the density present in C (cyan arrow) and D (cyan circle) is absent.

four classes were smaller and exhibited different tail and IHM structures in their reconstructions (Fig. 6, A, B, and E) and were therefore excluded from the final reconstruction.

The reason for the different 3-D classes is not certain. They might arise from variable staining of, and/or damage to, molecules caused during specimen preparation (e.g., stain drying). Alternatively, they could represent real variation in the structures of the molecules. When the tail can be traced clearly (classes 3, 4, and 6), the IHM shows more consistent structural features than in the other three classes. In these classes (30% of myosin molecules; classes 1, 2, and 5), the tail appeared flexible or disordered. Segment 2 density was discontinuous in class 1 and almost completely disappeared in classes 2 and 5, and the second hinge point was not visible in the latter two (Fig. 6, B and E). Although these classes exhibited a similar basic asymmetric organization of heads, their IHM structure was more varied, and the atomic model of the IHM (PDB ID 1I84) could not be docked into them very well. If the different classes represent real variation in the structures of the molecules, one of the possibilities suggested above, this would suggest that the tail could directly influence the stability of the molecules by strengthening the relatively weak interaction between the blocked and free heads. Disruption of tail interactions with the heads would then result in conformational changes and less compact myosin molecules.

Discussion

We have performed a 3-D reconstruction of the 10S conformation of myosin II. The reconstruction provides key insights into the likely mode of inhibition of myosin function through interactions of the tail with the heads. While the 3-D interactions between the heads that define the IHM in 10S myosin have been studied extensively by cryo-EM, only short fragments of the tail were visible and these provided no insight into the potential role of the tail in inhibition (Wendt et al., 2001; Liu et al., 2003; Hojjatian, 2019). In contrast, single particle negative stain studies of 10S myosin showed the full length of the tail (Burgess et al., 2007; Jung et al., 2008a,b, 2011). Negative staining was therefore our technique of choice for the work presented here. Our 2-D class averages were essentially identical to those of the earlier negative stain work (Burgess et al., 2007; Jung et al., 2008a,b, 2011), confirming that the entire path of the tail could be visualized, and that domains as small as 10 kD (e.g., the two lobes of the RLC) could be readily resolved in 2-D by this technique. The 2-D studies (Burgess et al., 2007) led to important proposals concerning the likely function of the tail, but lacked the 3-D insights provided by our reconstruction. Here, the organization and interactions of the tail with itself and the two heads are clearly seen in three dimensions (Fig. 3, D–F; and Video 2). The 25-Å resolution of the reconstruction (limited by flexibility of the molecule and the grain size of the stain; Burgess et al., 2004; Takizawa et al., 2017) was more than adequate to reveal the different domains of the myosin heavy chain and the 10-kD lobes of the light chains in 3-D (as with the 2-D class averages), and fitting the atomic model of the IHM (PDB ID 1I84) to the reconstruction can extend the effective resolution to better than 10 Å (Baker and Johnson, 1996; Fabiola and Chapman, 2005). The suggested interactions in this article, involving the subdomains of the heads with the tail, can be directly visualized in the map (Fig. S4), and some are supported by biochemical data. Although the reconstruction does not resolve interactions at the level of individual residues, this is not required to make reasonable conclusions about interactions between the heads and the tail at the subdomain level that provide strong clues as to how the molecule is switched off. Crucial functional insights at this resolution have been obtained in multiple other systems using negative staining (Vibert et al., 1997; Ohi et al., 2004; Takizawa et al., 2017).

The most important finding from our study is that interactions of the tail with the heads and with itself, combined with interactions between the heads, appear to block the four key functional characteristics of 10S myosin: (1) ATPase activity, by head–head and head–tail interaction; (2) actin binding, by head–head and head–tail interaction; (3) activation by phosphorylation, through RLC–tail interaction; and (4) filament formation, by tail–tail interaction. Inhibition of every aspect of myosin function appears to be nature's failsafe method for conserving energy in the inactive state.

Key tail interactions involved in switching off 10S myosin activity

The reconstruction shows evidence for eight possible interactions between the tail and the heads in 10S myosin (Table 1). Five

of these involve the blocked head, and three, the free head, suggesting that the blocked head is the more stable (Burgess et al., 2007). All eight interactions may be important in creating a fully inhibited 10S molecule, but two appear to be especially important.

Segment 1–blocked head interaction

Interaction between the blocked head and subfragment 2 (segment 1) of myosin (TB1; Fig. 5 B) appears to be one of the most fundamental interactions of the inhibited state, helping to maintain the blocked head in its folded-back conformation. This is suggested by its occurrence not only in myosin filaments and 10S myosin, but also in HMM (Burgess et al., 2007). In HMM, the free head preferentially detaches from the IHM in some molecules, while the blocked head remains bound to S2 (Burgess et al., 2007), suggesting preferential stabilization of the blocked head by this means. The free head also detaches more readily than the blocked head in 10S myosin (Burgess et al., 2007; Fig. S6) and filaments (Brito et al., 2011), further supporting stabilization of the blocked head by S2. Smooth muscle HMM constructs with different tail lengths are switched off only when the tail is at least as long as the head (Trybus et al., 1997). This is approximately the distance segment 1 must travel from its origin at the head–head junction to its interaction (TB1) with the blocked head mesa (Fig. 5 B), supporting the view that the S2–blocked head interaction plays a critical role in inhibition (Woodhead et al., 2005).

Segment 3–blocked-head RLC interaction

Interaction TB5, between segment 3 and the blocked-head RLC (Fig. 5 A), is supported by photo cross-linking, showing that Cys108, in the C-terminal half of the RLC, is cross-linked to the tail between Leu1554 and Glu1583, lying in segment 3 (Jung et al., 2011). The tail must therefore fold back on to the light chain domain. The calculated distance from Glu1535 to Lys1568 (the middle residue in the cross-linking region) is ∼48 Å, assuming 1.485-Å rise per residue along a coiled coil. In the reconstruction, the distance measured from Glu1535 (hinge 2; Burgess et al., 2007; star in Fig. 3 D) to Cys108 (cyan in Fig. 5, C and D; and Video 3) in the blocked-head RLC is similar (∼55 Å). In the cross-linking studies, only one of the two RLCs is cross-linked to the tail (Olney et al., 1996; Jung et al., 2011). This is readily explained by the reconstruction, which shows that only blocked head Cys108 is close enough to the tail for cross-linking (Video 3). Another cross-linking study suggests that sites on the N-lobes of both RLCs are close to the distal tail in the 10S structure (Salzameda et al., 2006). This is inconsistent with our reconstruction. Previous evidence suggests that the compact molecule is dynamic; thus, cross-linking may favor or trap a different conformer from the predominant form that we have studied (Salzameda et al., 2006; Jung et al., 2011). This would be consistent with the flexibility of the heads and tail suggested by the 3-D classification of our data discussed earlier (Fig. 6).

TB5 appears to be the most important interaction pinning the tail to the heads and creating the folded structure of 10S myosin. This is suggested by EM observations of 10S myosin. (1) When observed by rotary shadowing or negative staining, molecules that are not cross-linked by glutaraldehyde show a loosely folded structure, in which the only (therefore strongest) intramolecular contact occurs between the start of segment 3 and the neck region (containing the RLC) of one head (Craig et al., 1983; Jung et al., 2011). The other interactions in our reconstruction are presumably weaker and disrupted by binding of the molecule to the mica or carbon substrate used for imaging (Lee et al., 2018) when not stabilized by glutaraldehyde. (2) In *D. discoideum*and many insect flight muscle myosin II molecules, segment 3 does not bind to the blocked head; in these molecules, the tail and free head are correspondingly quite flexible (Fig. S6, A and C). (3) Segments 1 and 2 of smooth muscle myosin are together 1020 Å long (Burgess et al., 2007). Myosin IIs from amoeba (*Acanthamoeba castellanii*) and yeast (*Schizosaccharomyces pombe*) are much shorter, with total tail lengths of 870 and 910 Å, respectively (Lee et al., 2018). They thus lack segment 3 and the last 100–150 Å of segment 2. Neither of these myosins folds (Lee et al., 2018), consistent with the idea that segment 3/RLC interaction is essential for forming the 10S structure. (4) Biochemical and cell biological observations also support this view. The folded conformation fails to form when segments of the tail interacting with the RLC and the blocked head are replaced by skeletal sequences (Kiboku et al., 2013), or when the RLC is removed (Trybus and Lowey, 1988) or replaced by skeletal RLC (Trybus and Chatman, 1993). Experiments with chimeric smooth/skeletal RLCs show that native smooth N- and C-terminal lobes are both required for formation of 10S myosin (Trybus and Chatman, 1993)—the C-terminal lobe for full binding of the RLC to the heavy chain, and the N-terminal for folding. TB5 in our reconstruction shows segment 3 positioned over the C-terminal lobe and immediately next to the N-terminal lobe of the blocked-head RLC, providing a structural explanation for these findings (Fig. 7, E and F). The first 24 residues of the RLC are absent from the N-terminus in PDB ID 1I84, probably due to mobility. This region (the phosphorylation domain; Espinoza-Fonseca et al., 2008) stabilizes tail folding in smooth muscle myosin (Ikebe et al., 1994). We have estimated the location of these residues by superimposing the RLC of scallop (PDB ID 3JTD), which includes 11 additional N-terminal residues) on to the smooth muscle structure (Fig. S7). Residues 1–11 in scallop (14–24 in smooth muscle) of the blocked-head RLC appear to contact segment 3, consistent with this stabilizing interaction. Based on sequence analysis and modeling, it has been suggested that the N-terminal 24 amino acids, including a specific group of positively charged residues, may lie over a cluster of negatively charged residues in segment 3, trapping this region of the tail on top of the RLC C-lobe and accounting for the strength of this interaction (Jung et al., 2011). An alternative proposal is that these N-terminal RLC residues interact with helix A of the ELC in the switched-off molecule (Taylor et al., 2014). (5) The importance of blocked-head RLC–segment 3 interaction is also implied by the RLC Cys108 cross-linking studies referred to above. When cross-linked molecules are exposed to high salt, one head remains fully inhibited while the other has normal ATPase activity (Olney et al., 1996). This is consistent with our reconstruction. Cross-linking would maintain interaction of segment 3 with the RLC, which we suggest would help

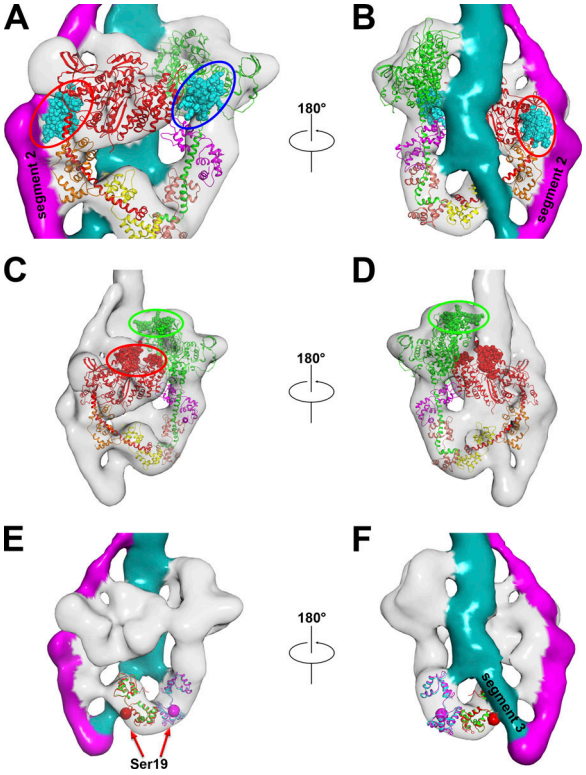

Figure 7. **Proposed inhibition mechanism of phosphate release and actin binding in the two heads. (A)** Phosphate release in the blocked head is inhibited by interaction of its converter domain (cyan within red ellipse) with segment 2, and in the free head by interaction of its converter domain (cyan within blue ellipse) with the blocked head. **(B)** Back view, rotated 180° from A. **(C and D)** Front and back views show actin-binding loop (red ellipse) in the blocked head sterically blocked by the free head, and actin-binding loop (green ellipse) in the free head blocked by interacting with the tail. **(E and F)** Front and back views showing steric blocking of Ser19 (red sphere) by segment 3 in the blocked-head RLC, but not in the free-head RLC (magenta sphere; see Video 4).

stabilize the inhibitory interactions of segment 2 with the blocked head. Free head interaction with the blocked head would be disrupted, thus activating the free head.

Other interactions

While the blocked-head RLC interacts with segment 3, a putative interaction (TF3) with the free-head RLC is less certain (Fig. 5, C and D). The density in this region is weak, and fitting of PDB ID 1I84 suggests that there is no RLC density to fill the volume (Fig. S4); the relatively uniform cylindrical tail also lacks such density (Figs. 4, 5, S3, and S4). This apparent interaction could represent low-resolution merging of the tail and head densities without actual contact. TF3 is close to the point where the first portion of segment 1, missing from the reconstruction, as discussed earlier (Figs. 3 E and S4), would meet segment 3. This may account for the sudden widening of the tail at this location (Fig. 5 B), leading to possible fusion with the RLC density.

In addition to interacting with the heads, the folded tail appears to interact with itself, where segments 1 and 3 run next to each other over the blocked head (interaction starting at TT2; Fig. 5 B), and at the top of the reconstruction, where all three segments form a compact, rod-shaped structure, extending upwards from TT1 (Figs. 3 and 5 A). These interactions appear to play an essential role in the function of 10S myosin. First, sequestering the tail inhibits polymerization with other tails to form filaments, the active form of myosin II in cells. Second, extending up from the TT1 contact site, the complex of the three tail segments is quite flexible and can be significantly curved (Burgess et al., 2007). However, the interacting-heads structure remains relatively rigid. The TT1 contact site may function as a lock, preventing conformational changes in the curved-rod complex from being transferred to the heads, thus helping to maintain their inhibited state. This is suggested by our observation that in the absence of TT1, as in *D. discoideum* (Fig. S6 B) and many insect indirect flight muscle myosin molecules (Fig. S6 D; Lee et al., 2018), the free head frequently detaches from the blocked head.

Tail segments 2 and 3 stabilize the IHM in 10S myosin

The atomic model of the IHM (PDB ID 1I84, based on 2-D crystals of HMM; Wendt et al., 2001) fits well into the head densities of the reconstruction, without the need for any substantial change in head structure (Fig. 4, D–F; and Video 2). This shows that binding of tail segments 2 and 3 (absent from HMM) to the heads in 10S myosin is not required to generate the head–head interactions, and that it does not significantly distort them. However, the frequency of formation of the interacting-heads structure, the stability of the free head, and the inhibition of activity are all lower in HMM than in 10S myosin (Burgess et al., 2007). Thus, segments 2 and 3 stabilize the head–head interactions and compact structure of 10S myosin, strengthening the inhibited state. Other data are consistent with this conclusion: (1) a subset of the reconstructions that lack some of the tail density features correspondingly had a more varied head structure (Fig. 6, A, B, and E); (2) myosin from *D. discoideum* (Lee et al., 2018), which lacks segment 2 wrapping around the blocked head (Lee et al., 2018), showed more frequent cases of noninteracting heads (Fig. S6, C and D); and (3) myosin molecules from insect flight muscle frequently behaved similarly (Fig. S6, A and B). These observations suggest that the interactions of all three tail segments with the heads are required to fully stabilize the 10S structure.

Comparison of intramolecular interactions in thick filaments and single molecules

10S myosin and thick filaments have several interactions in common (Table 1). Conservation of these interactions between filament and molecule suggests that they play an important role in the inhibited state. (1) In both filament and molecule, it is thought that the interaction between the two heads (BF) constrains movement of the converter domain of the free head, inhibiting phosphate release, and blocks actin binding by the blocked head (Wendt et al., 2001; Woodhead et al., 2005). (2) TB1 in 10S myosin occurs between tail segments 1 and/or 3 and the blocked head, where these two segments run over its motor domain (Fig. 5 B). In filaments, where the tail is not folded (Woodhead et al., 2005), and in HMM, where segments 2 and 3 are absent (Burgess et al., 2007; Jung et al., 2011), this interaction is also present, but can only involve S2, supporting the view that

TB1 involves S2 and consistent with data showing that subfragment 2 binds to subfragment 1 in solution (Nag et al., 2017). In 10S myosin, segment 3 may also be involved. The tail is wider where it runs over the blocked head than at the start of segment 3, where it is a single α-helix (Fig. 5 B), suggesting that segment 3 runs next to segment 1 over the blocked head. This double interaction with the blocked head may strengthen the stability of the IHM in the folded molecule. (3) TB2 (Fig. 5 A) occurs between segment 2 and the SH3 domain (blue in Fig. 5 A) of the blocked head. A related interaction is observed in relaxed thick filaments, between the SH3 domain of the blocked head and the tail from the next pair of heads away from the bare zone (Woodhead et al., 2005; Alamo et al., 2008); however, in this case the interaction involves segment 1, and its polarity is the reverse of that in the 10S molecule. (4) TB3 occurs between segment 2 and the converter domain of the blocked head (Fig. 5 A). As with TB2, a similar interaction (but with reverse polarity) occurs in thick filaments, between the converter domain and segment 1 of the neighboring tail (Woodhead et al., 2005). (5) The fifth interaction, TF1, occurs between tail segments 1 and/or 3 and the free head actin-binding loop in 10S myosin. A similar interaction between S2 and actin-binding loop 2 has been suggested in tarantula thick filaments (Alamo et al., 2016), suggesting that TF1 also involves S2.

Inhibition of 10S myosin by steric blocking of ATPase and actin-binding sites on both heads

Cryo-EM studies suggested that inhibition of 10S myosin through head–head interaction was achieved by different mechanisms in the two heads (Wendt et al., 2001; Liu et al., 2003): (1) by preventing actin binding in the blocked head and (2) by inhibiting ATPase activity in the free head (Wendt et al., 2001). But these studies provided no insight into the possible role of the tail in inhibition, as the tail was not clearly visualized. Our negative stain reconstruction suggests that the tail plays a central role in switching off activity, such that both of these inhibitory mechanisms occur in both heads, but in different ways.

Inhibition of actin binding

Part of the actin-binding interface of the blocked head is obstructed by interaction with the free head, as shown previously (Wendt et al., 2001; interaction BF, Fig. 5 A; red ellipse, Fig. 7 C). In the free head, it is clear that actin binding is also sterically blocked, through interaction of its actin-binding loop 2 with the tail (interaction TF1; Fig. 5 B; green ellipse in Fig. 7, C and D), and by interference of the bundle of three tail segments (projecting up from TT1) with the free head actin-binding interface. Thus, each head would be prevented from binding to actin by distinct steric blocking mechanisms, one involving the tail and one the other head. This is consistent with biochemical observations that the affinity of actin for 10S myosin is extremely weak (Ikebe and Hartshorne, 1986; Olney et al., 1996), suggesting that both heads are inhibited from binding to actin.

Inhibition of ATPase activity

Similarly, ATPase activity of 10S myosin appears to be inhibited not only in the free head, but also the blocked head, by stabilization of the converter domain of each, preventing phosphate release (compare Yount et al. [1995]). In the free head, the converter is immobilized by binding to the blocked head (Wendt et al., 2001; interaction BF, Fig. 5 A; blue ellipse, Fig. 7 A). In the blocked head, the converter may also be immobilized, in this case by binding to segment 2 of the tail as it wraps around the head (interaction TB3, Fig. 5 A; red ellipse, Fig. 7, A and B).

Inhibition of ATPase activity in both heads of 10S myosin would help explain a previously puzzling observation. Release of ATP hydrolysis products is 10 times slower in 10S myosin than in HMM (0.0002 s^{-1} and 0.003 s^{-1}, respectively; Cross et al., 1988). If the free head is inhibited in both (by binding to the blocked head), blocked-head product release must be more inhibited in 10S myosin than in HMM. This could be explained by interaction of tail segment 2 with the blocked head converter in 10S myosin but not HMM, where it is missing. As mentioned previously, tail wrapping around the heads may also stabilize the basic head–head interaction of the IHM (Wendt et al., 2001), enhancing the inhibitory effect of the two heads on each other in the 10S molecule.

We conclude that phosphate release and actin binding are both inhibited in both heads. This can explain why 10S myosin is completely switched off (Cross et al., 1988), making it so well suited to its proposed energy-conserving, storage function in cells. The folded tail plays a critical role in this inhibition.

In thick filaments (Woodhead et al., 2005), both actin binding and ATPase activity are also sterically inhibited in both heads, again in different ways. Blocked-head actin binding is inhibited by interacting with the free head, as with 10S myosin, while the free head is inhibited by orientation of its actin-binding face toward the thick filament backbone, away from actin. Both converters are also inhibited (Woodhead et al., 2005), impeding ATPase activity: in the free head by binding to the blocked head, as in 10S myosin; in the blocked head by interacting with S2 from the neighboring crown, as discussed above (Woodhead et al., 2005). The greater number of interactions found in 10S myosin than in thick filaments suggests that the IHM of 10S myosin is more stable than in thick filaments, consistent with the greater inhibition observed in molecules (Cross et al., 1988; Ankrett et al., 1991).

The role of the tail in activation of 10S myosin

Smooth and nonmuscle 10S myosins are activated in vitro by phosphorylation of their RLCs. Under physiological ionic conditions, this causes conversion to the 6S (unfolded) conformation (Craig et al., 1983; Trybus and Lowey, 1984), which can form filaments, hydrolyze ATP, and bind to actin. Our reconstruction provides some insights into the mechanisms of these processes. Biophysical data suggest that phosphorylation of 10S myosin is a sequential process, in which one RLC is phosphorylated more readily than the other, and it has been proposed that this might result from an asymmetric arrangement of the myosin heads (Persechini and Hartshorne, 1981, 1983; others have suggested that phosphorylation is random, but the starting myosin in those

studies may not have been in the 10S conformation (Trybus and Lowey, 1985; Wagner et al., 1985). The reconstruction reveals not only asymmetry of the heads (Wendt et al., 2001; Liu et al., 2003), but also dramatically different environments of their phosphorylation sites (due to the presence of the tail), which would readily account for a sequential phosphorylation process. Ser19 in the free-head RLC appears completely accessible to myosin light-chain kinase (MLCK) and would be easily phosphorylated. In the blocked head, Ser19 is sterically hindered by segment 3 of the tail (interaction TB5; Fig. 7, E and F; and Video 4), which would hamper access of MLCK. Thus, the free-head RLCs would be phosphorylated first, and blocked-head RLCs later (Persechini and Hartshorne, 1981, 1983; Ikebe et al., 1983a,b). A similar difference in accessibility of MLCK to the phosphorylatable serines is observed in tarantula filaments due to differing steric environments in the filament (Brito et al., 2011).

Biophysical measurements show that both RLCs must be phosphorylated for complete transition of the 10S to the 6S conformation (Ikebe et al., 1983a,b) and for significant activation of ATPase activity (Persechini and Hartshorne, 1981). This suggests that phosphorylation of the blocked-head RLC (occurring second) must ultimately determine unfolding, and that singly phosphorylated molecules would remain mostly folded and relatively inactive. The immediate proximity of Ser19 on the blocked-head RLC to interaction TB5, which we suggested earlier is the critical interaction for creating the folded state (Fig. 7, E and F), would explain how phosphorylation of this serine could be the key step that causes tail unfolding. This proximity suggests a direct (rather than allosteric) effect of phosphorylation on the binding of segment 3: decreased positive charge on the RLC would weaken its interaction with the negatively charged region of segment 3, favoring unfolding of the tail (Jung et al., 2011). Extension of RLC helix A upon phosphorylation (Espinoza-Fonseca et al., 2008), or changes in ELC–RLC interaction affecting the conformation of the light chain domain (Houdusse and Cohen, 1996; Taylor et al., 2014), might also contribute to the loss of interaction with segment 3. Importantly, HMM, which lacks segments 2 and 3, requires phosphorylation of only one of its two heads for activation (Walcott et al., 2009); in this case, TB5 does not exist, and phosphorylation of a single head is sufficient to break the weaker head–head interaction in HMM. The requirement for phosphorylation of both heads in 10S myosin (one of which is sterically inhibited) for full activation may be another mechanism by which the cell conserves energy in the quiescent state. If any MLCK molecules in the cell are Ca^{2+}-insensitive (e.g., through proteolysis or other damage), resulting RLC phosphorylation will occur preferentially on the free head, but this will not activate the molecule. Only when intracellular Ca^{2+} levels rise will there be sufficient activated MLCK to phosphorylate the blocked-head RLC as well, with concomitant unfolding of the 10S structure.

Based on the above observations and previous work, we propose the following mechanism for regulating 10S myosin activity in cells. (1) At low intracellular Ca^{2+}, both heads are dephosphorylated, and the molecule is in the 10S conformation, in which ATPase activity and actin binding are inhibited by the mechanisms discussed earlier. The compact structure (as either 10S monomers or small oligomers; Liu et al., 2017) would facilitate transport through the crowded intracellular environment, while inhibition of ATPase and actin binding would minimize energy use and futile binding to actin filaments during transport. (2) With increased Ca^{2+}, MLCK is activated and first phosphorylates the unobstructed RLC of the free head. This may alter the conformation of the light chain domain of this head, weakening interaction of the free head with the blocked head and the tail, while retaining the overall folded conformation and relatively low ATPase activity of the molecule (Persechini and Hartshorne, 1981; Ikebe et al., 1983a,b; Houdusse and Cohen, 1996; Burgess et al., 2007; Taylor et al., 2014). (3) The less accessible blocked-head RLC is then phosphorylated. This could result from the weakening of the IHM just mentioned, or from "breathing" of the intact 10S structure, which transiently exposes blocked head Ser19 (we assume that the interactions we have described are relatively weak and in equilibrium between interacting and noninteracting states). There is also evidence that the RLCs may interact with each other and with the flexible initial portion of subfragment 2, stabilizing the conformation of this region of the IHM (Woodhead et al., 2005, 2013; Alamo et al., 2008). Phosphorylation of the free-head RLC may disrupt these interactions, leading to increased local flexibility and greater accessibility of Ser19 on the blocked-head RLC. (4) Phosphorylation of the blocked-head phosphorylation domain weakens or abolishes its interaction (TB5) with the negative charge cluster on segment 3 due to decreased charge attraction. (5) With breakage of TB5 (the key interaction required for the folded state), the binding of segments 1 and 2 to the heads is destabilized, allowing the tail to become fully extended. (6) Loss of head–tail interactions during tail unfolding may further destabilize previously weakened head–head contacts, promoting separation of the heads. (7) The extended tails now interact to form filaments, actin-binding sites on both heads are exposed, and inhibitory interactions of the converter domains are lifted, leading to full actin-activated ATPase activity and filament sliding.

Acknowledgments

Henk L. Granzier served as editor.

We thank Drs. Edward Korn and Xiong Liu (National Heart, Lung, and Blood Institute, Bethesda, MD) for *D. discoideum* myosin and Sanford Bernstein and Floyd Sarsoza (San Diego State University, San Diego, CA) for insect flight muscle myosin. We thank the Electron Microscopy Facility and its staff (Dr. Gregory Hendricks, Dr. Lara Strittmatter, and Keith Reddig) at University of Massachusetts Medical School for instrumentation and assistance.

This work was supported by National Institutes of Health grants AR072036, AR067279, and HL139883 (R. Craig) and HL075030 and HL111696 (M. Ikebe). M. Ikebe is an awardee of University of Texas STARS PLUS Award. The content is solely the responsibility of the authors and does not necessarily represent the official views of the National Institutes of Health.

The authors declare no competing financial interests.

Author contributions: S. Yang carried out the image analysis, 3-D reconstruction, and atomic fitting; analyzed the results; reviewed the literature; and wrote the first draft of the paper. K.H. Lee carried out the electron microscopy. J.L. Woodhead contributed to analysis of the reconstruction and writing of the paper. O. Sato prepared the myosin. M. Ikebe contributed to writing of the paper and funding acquisition. R. Craig wrote later drafts of the paper, provided overall conceptualization, and contributed to analysis of the results and funding acquisition.

Submitted: 26 June 2019
Accepted: 8 July 2019

References

Alamo, L., W. Wriggers, A. Pinto, F. Bártoli, L. Salazar, F.Q. Zhao, R. Craig, and R. Padrón. 2008. Three-dimensional reconstruction of tarantula myosin filaments suggests how phosphorylation may regulate myosin activity. *J. Mol. Biol.* 384:780–797. https://doi.org/10.1016/j.jmb.2008.10.013

Alamo, L., D. Qi, W. Wriggers, A. Pinto, J. Zhu, A. Bilbao, R.E. Gillilan, S. Hu, and R. Padrón. 2016. Conserved Intramolecular Interactions Maintain Myosin Interacting-Heads Motifs Explaining Tarantula Muscle Super-Relaxed State Structural Basis. *J. Mol. Biol.* 428:1142–1164. https://doi.org/10.1016/j.jmb.2016.01.027

Ankrett, R.J., A.J. Rowe, R.A. Cross, J. Kendrick-Jones, and C.R. Bagshaw. 1991. A folded (10 S) conformer of myosin from a striated muscle and its implications for regulation of ATPase activity. *J. Mol. Biol.* 217:323–335. https://doi.org/10.1016/0022-2836(91)90546-I

Baker, T.S., and J.E. Johnson. 1996. Low resolution meets high: towards a resolution continuum from cells to atoms. *Curr. Opin. Struct. Biol.* 6: 585–594. https://doi.org/10.1016/S0959-440X(96)80023-6

Breckenridge, M.T., N.G. Dulyaninova, and T.T. Egelhoff. 2009. Multiple regulatory steps control mammalian nonmuscle myosin II assembly in live cells. *Mol. Biol. Cell.* 20:338–347. https://doi.org/10.1091/mbc.e08-04-0372

Brito, R., L. Alamo, U. Lundberg, J.R. Guerrero, A. Pinto, G. Sulbarán, M.A. Gawinowicz, R. Craig, and R. Padrón. 2011. A molecular model of phosphorylation-based activation and potentiation of tarantula muscle thick filaments. *J. Mol. Biol.* 414:44–61. https://doi.org/10.1016/j.jmb.2011.09.017

Brown, J.H., Y. Yang, L. Reshetnikova, S. Gourinath, D. Süveges, J. Kardos, F. Hóbor, R. Reutzel, L. Nyitray, and C. Cohen. 2008. An unstable head-rod junction may promote folding into the compact off-state conformation of regulated myosins. *J. Mol. Biol.* 375:1434–1443. https://doi.org/10.1016/j.jmb.2007.11.071

Burgess, S.A., M.L. Walker, K. Thirumurugan, J. Trinick, and P.J. Knight. 2004. Use of negative stain and single-particle image processing to explore dynamic properties of flexible macromolecules. *J. Struct. Biol.* 147:247–258. https://doi.org/10.1016/j.jsb.2004.04.004

Burgess, S.A., S. Yu, M.L. Walker, R.J. Hawkins, J.M. Chalovich, and P.J. Knight. 2007. Structures of smooth muscle myosin and heavy meromyosin in the folded, shutdown state. *J. Mol. Biol.* 372:1165–1178. https://doi.org/10.1016/j.jmb.2007.07.014

Craig, R., R. Smith, and J. Kendrick-Jones. 1983. Light-chain phosphorylation controls the conformation of vertebrate non-muscle and smooth muscle myosin molecules. *Nature.* 302:436–439. https://doi.org/10.1038/302436a0

Cross, R.A. 1988. What is 10S myosin for? *J. Muscle Res. Cell Motil.* 9:108–110. https://doi.org/10.1007/BF01682153

Cross, R.A., K.E. Cross, and A. Sobieszek. 1986. ATP-linked monomer-polymer equilibrium of smooth muscle myosin: the free folded monomer traps ADP.Pi. *EMBO J.* 5:2637–2641. https://doi.org/10.1002/j.1460-2075.1986.tb04545.x

Cross, R.A., A.P. Jackson, S. Citi, J. Kendrick-Jones, and C.R. Bagshaw. 1988. Active site trapping of nucleotide by smooth and non-muscle myosins. *J. Mol. Biol.* 203:173–181. https://doi.org/10.1016/0022-2836(88)90100-3

Espinoza-Fonseca, L.M., D. Kast, and D.D. Thomas. 2008. Thermodynamic and structural basis of phosphorylation-induced disorder-to-order transition in the regulatory light chain of smooth muscle myosin. *J. Am. Chem. Soc.* 130:12208–12209. https://doi.org/10.1021/ja803143g

Fabiola, F., and M.S. Chapman. 2005. Fitting of high-resolution structures into electron microscopy reconstruction images. *Structure.* 13:389–400. https://doi.org/10.1016/j.str.2005.01.007

Frank, J. 2006. *Three-dimensional electron microscopy of macromolecular assemblies: visualization of biological molecules in their native state.* Second edition. Oxford University Press, Oxford, UK. 410 pp. https://doi.org/10.1093/acprof:oso/9780195182187.001.0001

Geeves, M.A., and K.C. Holmes. 1999. Structural mechanism of muscle contraction. *Annu. Rev. Biochem.* 68:687–728. https://doi.org/10.1146/annurev.biochem.68.1.687

Heissler, S.M., and J.R. Sellers. 2016. Various Themes of Myosin Regulation. *J. Mol. Biol.* 428(9, 9 Pt B):1927–1946.

Hojjatian, A. 2019. CryoEM single particle reconstruction of dephosphorylated HMM from smooth muscle. *Biophys. J.* 116(3, suppl 1):406A. https://doi.org/10.1016/j.bpj.2018.11.2193

Houdusse, A., and C. Cohen. 1996. Structure of the regulatory domain of scallop myosin at 2 A resolution: implications for regulation. *Structure.* 4:21–32. https://doi.org/10.1016/S0969-2126(96)00006-8

Ikebe, M., and D.J. Hartshorne. 1985. Effects of Ca2+ on the conformation and enzymatic activity of smooth muscle myosin. *J. Biol. Chem.* 260: 13146–13153.

Ikebe, M., and D.J. Hartshorne. 1986. Proteolysis and actin-binding properties of 10S and 6S smooth muscle myosin: identification of a site protected from proteolysis in the 10S conformation and by the binding of actin. *Biochemistry.* 25:6177–6185. https://doi.org/10.1021/bi00368a052

Ikebe, M., S. Hinkins, and D.J. Hartshorne. 1983a. Correlation of enzymatic properties and conformation of smooth muscle myosin. *Biochemistry.* 22:4580–4587. https://doi.org/10.1021/bi00288a036

Ikebe, M., S. Hinkins, and D.J. Hartshorne. 1983b. Correlation of intrinsic fluorescence and conformation of smooth muscle myosin. *J. Biol. Chem.* 258:14770–14773.

Ikebe, M., R. Ikebe, H. Kamisoyama, S. Reardon, J.P. Schwonek, C.R. Sanders II, and M. Matsuura. 1994. Function of the NH2-terminal domain of the regulatory light chain on the regulation of smooth muscle myosin. *J. Biol. Chem.* 269:28173–28180.

Jung, H.S., S.A. Burgess, N. Billington, M. Colegrave, H. Patel, J.M. Chalovich, P.D. Chantler, and P.J. Knight. 2008a. Conservation of the regulated structure of folded myosin 2 in species separated by at least 600 million years of independent evolution. *Proc. Natl. Acad. Sci. USA.* 105: 6022–6026. https://doi.org/10.1073/pnas.0707846105

Jung, H.S., S. Komatsu, M. Ikebe, and R. Craig. 2008b. Head-head and head-tail interaction: a general mechanism for switching off myosin II activity in cells. *Mol. Biol. Cell.* 19:3234–3242. https://doi.org/10.1091/mbc.e08-02-0206

Jung, H.S., N. Billington, K. Thirumurugan, B. Salzameda, C.R. Cremo, J.M. Chalovich, P.D. Chantler, and P.J. Knight. 2011. Role of the tail in the regulated state of myosin 2. *J. Mol. Biol.* 408:863–878. https://doi.org/10.1016/j.jmb.2011.03.019

Katoh, T., K. Konishi, and M. Yazawa. 1998. Skeletal muscle myosin monomer in equilibrium with filaments forms a folded conformation. *J. Biol. Chem.* 273:11436–11439. https://doi.org/10.1074/jbc.273.19.11436

Kiboku, T., T. Katoh, A. Nakamura, A. Kitamura, M. Kinjo, Y. Murakami, and M. Takahashi. 2013. Nonmuscle myosin II folds into a 10S form via two portions of tail for dynamic subcellular localization. *Genes Cells.* 18: 90–109. https://doi.org/10.1111/gtc.12021

Lee, K.H., G. Sulbarán, S. Yang, J.Y. Mun, L. Alamo, A. Pinto, O. Sato, M. Ikebe, X. Liu, E.D. Korn, et al. 2018. Interacting-heads motif has been conserved as a mechanism of myosin II inhibition since before the origin of animals. *Proc. Natl. Acad. Sci. USA.* 115:E1991–E2000. https://doi.org/10.1073/pnas.1715247115

Liu, J., T. Wendt, D. Taylor, and K. Taylor. 2003. Refined model of the 10S conformation of smooth muscle myosin by cryo-electron microscopy 3D image reconstruction. *J. Mol. Biol.* 329:963–972. https://doi.org/10.1016/S0022-2836(03)00516-3

Liu, X., N. Billington, S. Shu, S.H. Yu, G. Piszczek, J.R. Sellers, and E.D. Korn. 2017. Effect of ATP and regulatory light-chain phosphorylation on the polymerization of mammalian nonmuscle myosin II. *Proc. Natl. Acad. Sci. USA.* 114:E6516–E6525. https://doi.org/10.1073/pnas.1702375114

Milton, D.L., A.N. Schneck, D.A. Ziech, M. Ba, K.C. Facemyer, A.J. Halayko, J.E. Baker, W.T. Gerthoffer, and C.R. Cremo. 2011. Direct evidence for functional smooth muscle myosin II in the 10S self-inhibited monomeric conformation in airway smooth muscle cells. *Proc. Natl. Acad. Sci. USA.* 108:1421–1426. https://doi.org/10.1073/pnas.1011784108

Moore, J.R., L. Leinwand, and D.M. Warshaw. 2012. Understanding cardiomyopathy phenotypes based on the functional impact of mutations in

the myosin motor. *Circ. Res.* 111:375–385. https://doi.org/10.1161/CIRCRESAHA.110.223842

Nag, S., D.V. Trivedi, S.S. Sarkar, A.S. Adhikari, M.S. Sunitha, S. Sutton, K.M. Ruppel, and J.A. Spudich. 2017. The myosin mesa and the basis of hypercontractility caused by hypertrophic cardiomyopathy mutations. *Nat. Struct. Mol. Biol.* 24:525–533. https://doi.org/10.1038/nsmb.3408

Newell-Litwa, K.A., R. Horwitz, and M.L. Lamers. 2015. Non-muscle myosin II in disease: mechanisms and therapeutic opportunities. *Dis. Model. Mech.* 8:1495–1515. https://doi.org/10.1242/dmm.022103

Ohi, M., Y. Li, Y. Cheng, and T. Walz. 2004. Negative Staining and Image Classification - Powerful Tools in Modern Electron Microscopy. *Biol. Proced. Online.* 6:23–34. https://doi.org/10.1251/bpo70

Olney, J.J., J.R. Sellers, and C.R. Cremo. 1996. Structure and function of the 10 S conformation of smooth muscle myosin. *J. Biol. Chem.* 271: 20375–20384. https://doi.org/10.1074/jbc.271.34.20375

Persechini, A., and D.J. Hartshorne. 1981. Phosphorylation of smooth muscle myosin: evidence for cooperativity between the myosin heads. *Science.* 213:1383–1385. https://doi.org/10.1126/science.6455737

Persechini, A., and D.J. Hartshorne. 1983. Ordered phosphorylation of the two 20 000 molecular weight light chains of smooth muscle myosin. *Biochemistry.* 22:470–476. https://doi.org/10.1021/bi00271a033

Pettersen, E.F., T.D. Goddard, C.C. Huang, G.S. Couch, D.M. Greenblatt, E.C. Meng, and T.E. Ferrin. 2004. UCSF Chimera--a visualization system for exploratory research and analysis. *J. Comput. Chem.* 25:1605–1612. https://doi.org/10.1002/jcc.20084

Pinto, A., F. Sánchez, L. Alamo, and R. Padrón. 2012. The myosin interacting-heads motif is present in the relaxed thick filament of the striated muscle of scorpion. *J. Struct. Biol.* 180:469–478. https://doi.org/10.1016/j.jsb.2012.08.010

Radermacher, M., T. Wagenknecht, A. Verschoor, and J. Frank. 1987. Three-dimensional reconstruction from a single-exposure, random conical tilt series applied to the 50S ribosomal subunit of Escherichia coli. *J. Microsc.* 146:113–136. https://doi.org/10.1111/j.1365-2818.1987.tb01333.x

Salzameda, B., K.C. Facemyer, B.W. Beck, and C.R. Cremo. 2006. The N-terminal lobes of both regulatory light chains interact with the tail domain in the 10 S-inhibited conformation of smooth muscle myosin. *J. Biol. Chem.* 281:38801–38811. https://doi.org/10.1074/jbc.M606555200

Scheres, S.H. 2012. RELION: implementation of a Bayesian approach to cryo-EM structure determination. *J. Struct. Biol.* 180:519–530. https://doi.org/10.1016/j.jsb.2012.09.006

Sellers, J.R. 1991. Regulation of cytoplasmic and smooth muscle myosin. *Curr. Opin. Cell Biol.* 3:98–104. https://doi.org/10.1016/0955-0674(91)90171-T

Seow, C.Y. 2005. Myosin filament assembly in an ever-changing myofilament lattice of smooth muscle. *Am. J. Physiol. Cell Physiol.* 289: C1363–C1368. https://doi.org/10.1152/ajpcell.00329.2005

Shutova, M.S., and T.M. Svitkina. 2018. Mammalian nonmuscle myosin II comes in three flavors. *Biochem. Biophys. Res. Commun.* 506:394–402. https://doi.org/10.1016/j.bbrc.2018.03.103

Spudich, J.A. 2015. The myosin mesa and a possible unifying hypothesis for the molecular basis of human hypertrophic cardiomyopathy. *Biochem. Soc. Trans.* 43:64–72. https://doi.org/10.1042/BST20140324

Stewart, M.A., K. Franks-Skiba, S. Chen, and R. Cooke. 2010. Myosin ATP turnover rate is a mechanism involved in thermogenesis in resting skeletal muscle fibers. *Proc. Natl. Acad. Sci. USA.* 107:430–435. https://doi.org/10.1073/pnas.0909468107

Suzuki, H., H. Onishi, K. Takahashi, and S. Watanabe. 1978. Structure and function of chicken gizzard myosin. *J. Biochem.* 84:1529–1542. https://doi.org/10.1093/oxfordjournals.jbchem.a132278

Suzuki, H., T. Kamata, H. Onishi, and S. Watanabe. 1982. Adenosine triphosphate-induced reversible change in the conformation of chicken gizzard myosin and heavy meromyosin. *J. Biochem.* 91:1699–1705. https://doi.org/10.1093/oxfordjournals.jbchem.a133861

Tajsharghi, H., and A. Oldfors. 2013. Myosinopathies: pathology and mechanisms. *Acta Neuropathol.* 125:3–18. https://doi.org/10.1007/s00401-012-1024-2

Takahashi, T., C. Fukukawa, C. Naraoka, T. Katoh, and M. Yazawa. 1999. Conformations of vertebrate striated muscle myosin monomers in equilibrium with filaments. *J. Biochem.* 126:34–40. https://doi.org/10.1093/oxfordjournals.jbchem.a022433

Takizawa, Y., E. Binshtein, A.L. Erwin, T.M. Pyburn, K.F. Mittendorf, and M.D. Ohi. 2017. While the revolution will not be crystallized, biochemistry reigns supreme. *Protein Sci.* 26:69–81. https://doi.org/10.1002/pro.3054

Tang, G., L. Peng, P.R. Baldwin, D.S. Mann, W. Jiang, I. Rees, and S.J. Ludtke. 2007. EMAN2: an extensible image processing suite for electron microscopy. *J. Struct. Biol.* 157:38–46. https://doi.org/10.1016/j.jsb.2006.05.009

Taylor, K.A., M. Feig, C.L. Brooks III, P.M. Fagnant, S. Lowey, and K.M. Trybus. 2014. Role of the essential light chain in the activation of smooth muscle myosin by regulatory light chain phosphorylation. *J. Struct. Biol.* 185:375–382. https://doi.org/10.1016/j.jsb.2013.12.008

Trybus, K.M., and T.A. Chatman. 1993. Chimeric regulatory light chains as probes of smooth muscle myosin function. *J. Biol. Chem.* 268:4412–4419.

Trybus, K.M., and S. Lowey. 1984. Conformational states of smooth muscle myosin. Effects of light chain phosphorylation and ionic strength. *J. Biol. Chem.* 259:8564–8571.

Trybus, K.M., and S. Lowey. 1985. Mechanism of smooth muscle myosin phosphorylation. *J. Biol. Chem.* 260:15988–15995.

Trybus, K.M., and S. Lowey. 1988. The regulatory light chain is required for folding of smooth muscle myosin. *J. Biol. Chem.* 263:16485–16492.

Trybus, K.M., T.W. Huiatt, and S. Lowey. 1982. A bent monomeric conformation of myosin from smooth muscle. *Proc. Natl. Acad. Sci. USA.* 79: 6151–6155. https://doi.org/10.1073/pnas.79.20.6151

Trybus, K.M., Y. Freyzon, L.Z. Faust, and H.L. Sweeney. 1997. Spare the rod, spoil the regulation: necessity for a myosin rod. *Proc. Natl. Acad. Sci. USA.* 94:48–52. https://doi.org/10.1073/pnas.94.1.48

Urnavicius, L., K. Zhang, A.G. Diamant, C. Motz, M.A. Schlager, M. Yu, N.A. Patel, C.V. Robinson, and A.P. Carter. 2015. The structure of the dynactin complex and its interaction with dynein. *Science.* 347:1441–1446. https://doi.org/10.1126/science.aaa4080

Vibert, P., R. Craig, and W. Lehman. 1997. Steric-model for activation of muscle thin filaments. *J. Mol. Biol.* 266:8–14. https://doi.org/10.1006/jmbi.1996.0800

Vicente-Manzanares, M., X. Ma, R.S. Adelstein, and A.R. Horwitz. 2009. Non-muscle myosin II takes centre stage in cell adhesion and migration. *Nat. Rev. Mol. Cell Biol.* 10:778–790. https://doi.org/10.1038/nrm2786

Wagner, P.D., N.D. Vu, and J.N. George. 1985. Random phosphorylation of the two heads of thymus myosin and the independent stimulation of their actin-activated ATPases. *J. Biol. Chem.* 260:8084–8089.

Walcott, S., P.M. Fagnant, K.M. Trybus, and D.M. Warshaw. 2009. Smooth muscle heavy meromyosin phosphorylated on one of its two heads supports force and motion. *J. Biol. Chem.* 284:18244–18251. https://doi.org/10.1074/jbc.M109.003293

Wendt, T., D. Taylor, K.M. Trybus, and K. Taylor. 2001. Three-dimensional image reconstruction of dephosphorylated smooth muscle heavy meromyosin reveals asymmetry in the interaction between myosin heads and placement of subfragment 2. *Proc. Natl. Acad. Sci. USA.* 98: 4361–4366. https://doi.org/10.1073/pnas.071051098

Woodhead, J.L., F.Q. Zhao, R. Craig, E.H. Egelman, L. Alamo, and R. Padrón. 2005. Atomic model of a myosin filament in the relaxed state. *Nature.* 436:1195–1199. https://doi.org/10.1038/nature03920

Woodhead, J.L., F.Q. Zhao, and R. Craig. 2013. Structural basis of the relaxed state of a Ca2+-regulated myosin filament and its evolutionary implications. *Proc. Natl. Acad. Sci. USA.* 110:8561–8566. https://doi.org/10.1073/pnas.1218462110

Xu, J.Q., J.M. Gillis, and R. Craig. 1997. Polymerization of myosin on activation of rat anococcygeus smooth muscle. *J. Muscle Res. Cell Motil.* 18:381–393. https://doi.org/10.1023/A:1018634412117

Yang, S., J.L. Woodhead, F.Q. Zhao, G. Sulbarán, and R. Craig. 2016. An approach to improve the resolution of helical filaments with a large axial rise and flexible subunits. *J. Struct. Biol.* 193:45–54. https://doi.org/10.1016/j.jsb.2015.11.007

Yount, R.G., D. Lawson, and I. Rayment. 1995. Is myosin a "back door" enzyme? *Biophys. J.* 68(4, Suppl):44S–47S, discussion:47S–49S.

Zhao, F.Q., R. Craig, and J.L. Woodhead. 2009. Head-head interaction characterizes the relaxed state of Limulus muscle myosin filaments. *J. Mol. Biol.* 385:423–431. https://doi.org/10.1016/j.jmb.2008.10.038

Zoghbi, M.E., J.L. Woodhead, R.L. Moss, and R. Craig. 2008. Three-dimensional structure of vertebrate cardiac muscle myosin filaments. *Proc. Natl. Acad. Sci. USA.* 105:2386–2390. https://doi.org/10.1073/pnas.0708912105